

## **A Modelling Approach to Evaluate Preliminary Remote Sensing Algorithms: Use of Water Quality Data from Swedish Great Lakes**

*Donald C. Pierson and Niklas Strömbeck*

Dept of Limnology, Inst. of Evolutionary Biology, Uppsala University,  
Norbyvägen 20, S 752 36 Uppsala Sweden

(Received: May 2000; Accepted: October 2000)

### *Abstract*

*There is presently an extensive long term data base of water quality parameters (<http://www.ma.slu.se>) for Lakes Vänern (1973–present), Lake Vättern (1966–present), and Lake Mälaren (1966–Present). These data were used to estimate variations in the concentrations of chlorophyll, dissolved yellow substances, and suspended particulate inorganic material (SPIM) in the upper water layer of each lake, which were in turn used to drive a simple model of in-water optics which predicted water leaving radiance reflectance. Simulations which randomly varied the optically active substances based on their frequency distributions were used to produce synthetic data sets which realistically simulated the variability in radiance reflectance and which could be used to examine the possible remote sensing algorithms which could be applied to each lake.*

*Most accurate estimates of SPIM were obtained from a linear relationship with radiance reflectance at wavelengths greater than 600 nm ( $r^2$  value exceeding 0.9 in all lakes). The absorption of yellow substances at 420 nm ( $a_y$  420) was predictable by linear regression against a band ratio of a wavelength > 600 nm to a wavelength in the 400–580 nm range. ( $r^2$  value exceeding 0.8 in all lakes). However, in Lake Mälaren, the strongest  $a_y$  algorithms were obtained when the numerator of the band ratio was within the phytoplankton pigment absorption peak between 600–700 nm. Estimation of chlorophyll depended on measuring a decrease in reflectance brought about by the chlorophyll absorption peak between 660–680 nm. The ratio of a band at a wavelength greater than 700 nm to a band within the red chlorophyll absorption peak yields acceptable estimates of chlorophyll ( $r^2$  value exceeding 0.6 in all lakes). Simulations of radiance reflectance in the MERIS sensor bands showed that SPIM was best estimated from band 9 (705 nm). The concentrations of chlorophyll and  $a_y$ (420) were best estimated from the band ratios 9/7 (705 nm/665 nm) and 7/3 (665 nm/490 nm) respectively. These results suggest that MERIS band 7 will play a crucial role in providing accurate estimate of chlorophyll and dissolved yellow substances in Swedish freshwaters.*

*Key words: Remote sensing, water quality, optics, model, chlorophyll, MERIS*

### *1. Introduction*

In order to develop remote sensing algorithms for the use with various satellite sensors a commonly applied approach is to collect data simultaneously with a satellite overpass and then develop correlations between the satellite measured reflectance or

radiance and the optically active substances in the water (see *Lindell et al.*, 1999 for a review of this methodology as applied to lakes). One disadvantage with this method is that the logistics of obtaining data simultaneously with the satellite overpass can be demanding and as a result the data base for calibration can be limited in time and space (this is not always the case see *O'Reilly et al.*, 1998). In many cases therefore, the algorithms developed will be limited to the conditions under which the calibration data were collected, and may not be generally applicable to the water body at all times of interest.

An alternative to the above approach is to develop synthetic data sets through the use of optical modelling and then develop algorithms based on these synthetic data. The advantages of this method are that it is quick and relatively inexpensive to apply, and that realistic variations in radiance reflectance can be simulated if the variability in optically active concentrations is well understood. The synthetic data sets generated can be examined either at hyperspectral resolution or at the band widths of present or planned remote sensing sensors, allowing optimal sensor, and sensor specific evaluations to be made. Of course, the accuracy of this method will be dependent on the accuracy of the models used and, therefore, care must be taken to calibrate the model to the water body of interest. Furthermore, attention must be paid to the accuracy and variability in model parameterization (*Pierson and Strömbeck*, 2000). Here we present the results of a pilot study which took the modelling approach to screen present and future satellite sensors, and develop preliminary remote sensing algorithms for Lakes Vättern, Vänern and Mälaren, Sweden's three largest lakes. And, in doing so we demonstrate the use of models of aquatic optics as a screening tool for sensor evaluation and algorithm development. To estimating the variability in the optically active substances in each lake we made use of an extensive (greater than 25 year) data base of water quality parameters collected by the Swedish Environmental Protection Agency. These data allow the frequency distributions of optically active substances in each lake to be defined with an unusual degree of certainty, and therefore allow the simulation of radiance reflectance over a realistic range of variation.

## 2. *Methods*

### 2.1 *Modelling*

The model used for simulating radiance reflectance is similar to that described by *Pierson and Strömbeck* (2001) and *Strömbeck and Pierson* (2001). Like most other simple semi-analytical models (e.g. *Gordon et al.*, 1988; *Sathyendranath et al.*, 1989), irradiance reflectance ( $E_u/E_d$ ) or radiance reflectance ( $L_u/E_d$ ) is predicted as a function of the concentrations of optically active substances in the water. These model inputs include the concentrations of chlorophyll *a* + phaeophytin *a* (Chl), suspended particular inorganic material (SPIM), and dissolved yellow substances ( $a_y(420)$ ). Subsequently, these substances are linked to two key inherent optical properties (IOPs) of the water,

the absorption ( $a$ ) and backscattering ( $b_b$ ) coefficients through a series of empirical relationships that allow spectral variations in  $a(\lambda)$  and  $b_b(\lambda)$  to be estimated. Ultimately, radiance reflectance is estimated as a function of the ratio of backscattering to absorption. The input value representing the concentration of dissolved yellow substances is  $a_y(420)$ , which is in fact an IOP. For our purposes  $a_y(420)$  was also considered as an input variable, since it is a measurement of yellow substances which is available from historical data sets. In this case parameterization of the model involved transforming the single value of  $a_y(420)$  into the spectral variations in  $a_y(\lambda)$ , rather than estimating  $a_y(\lambda)$  from an independent concentration.

We define our model's parameterization as: the equations and constants, comprising the model, which transform the optically active concentrations to an output spectra of radiance reflectance. Parameterization is based on *in situ* measurements and laboratory analysis of both the optically active concentrations and the inherent optical properties (IOPs) of Lake Mälaren water, and in Lake Mälaren the model has been shown to reproduce measured variations in radiance reflectance with a good degree of accuracy, (Pierson and Strömbeck, 2001; Strömbeck and Pierson, 2001). As such, the model is most applicable to Lake Mälaren; however, variations in the optically active concentrations and the IOPs in Mälaren encompass the variability found in both Vänern and Vättern, suggesting that the Mälaren parameterization can reasonably be applied to all three lakes. Clearly, more accurate estimates of radiance reflectance would be obtained if lake specific parameterization for Vänern and Vättern were used. However, the point of this paper is to demonstrate the use of modelling as a rapid screening tool to evaluate *preliminary* remote sensing algorithms. In such a case it is appropriate to base model parameterization on non site specific data. The model was run between the wavelengths of 400–750 nm, and it is assumed that the water column is homogeneously mixed, so that neither the IOPs nor the estimated radiance reflectance vary with depth. A schematic overview of our model is shown in Figure 1. Details concerning the parameterization of the model are described below.

The total absorption coefficient ( $m^{-1}$ ) can be devolved into four additive coefficients which describe the absorption of water yellow substances, detrital material and phytoplankton.

$$a(\lambda) = a_w(\lambda) + a_y(\lambda) + a_d(\lambda) + a_{ph}(\lambda) \quad (1)$$

In order to calculate  $a_{ph}$  we make use of the relationship described in *Bricaud et al.* (1995) which predicts the chlorophyll specific phytoplankton absorption coefficient ( $a_{ph}^*$ ) as

$$a_{ph}^*(\lambda) = A(\lambda)Chl^{-B(\lambda)} \quad (2)$$

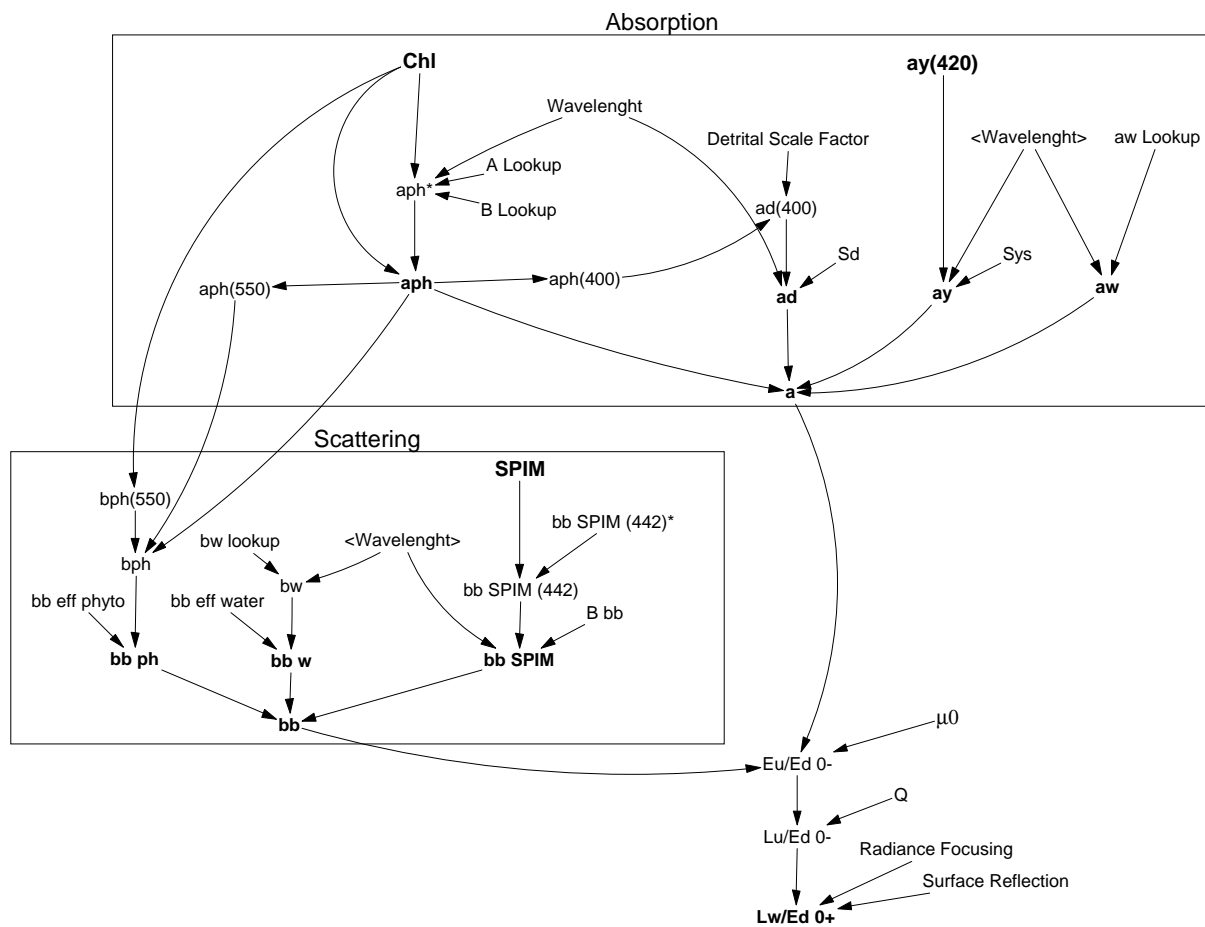


Fig. 1. Schematic diagram of the optical model. The optically active substances which drive the model are Chl,  $a_y(420)$  and SPIM (shown in large bold type). The output of the model is water leaving radiance reflectance ( $L_w/E_d 0+$ ) shown at the bottom of the diagram.

The spectra coefficients A and B are estimated from measurements made in Lake Mälaren as described below. The phytoplankton absorption coefficient is then calculated as

$$a_{ph}(\lambda) = a_{ph}^*(\lambda)Chl \quad (3)$$

The absorption spectra of dissolved yellow substances was calculated according to the Equation (4), where  $S_y$  is a shape factor (e.g., *Bricaud et al.*, 1981 or *Nelson and Guarda*, 1995).

$$a_y(\lambda) = a_y(400) e^{-S_y(\lambda-400)} \quad (4)$$

Detrital absorption at 400 nm is set to a fixed multiple (3.44) of the phytoplankton absorption at 400 nm. This constant is defined as the Detrital Scale Factor in Fig. 1 and  $a_d(400)$  is subsequently calculated as the product of  $a_{ph}(400)$  and the Detrital Scale Factor. The value of the detrital scale factor is based on measurements in Lake Mälaren when both  $a_d(400)$  and  $a_{ph}(400)$  were independently estimated (Table 1). The assump-

tion that detrital absorption is fixed proportion of phytoplankton absorption is clearly an oversimplification that must lead to some inaccuracy in the modelled radiance reflectance. Luckily,  $a_y$  is usually much greater than  $a_d$  (Table 2) so that some error in  $a_d$  is acceptable. In other studies (*Pierson and Strömbeck, 2001; Strömbeck and Pierson, 2001*) we have predicted detrital absorption as a function of concentrations of suspended particulate organic material (SPOM). This parameter has not however, been measured in the long term data sets for the Swedish Great Lakes, so we are forced to base detrital absorption on that simulated for the phytoplankton in order to utilise these valuable long term data sets.

Table 1. Model parameter values used in all simulations.

Parameter	Value	Source
$A(\lambda)$	Lookup Table	Derived from field measurements Lake Mälaren 1997
$B(\lambda)$	Lookup Table	Field measurements
$S_y$	0.014	Field measurements
$S_d$	0.0114	Field measurements
$Bb_b$	1.72	Field measurements
$b_{b\text{ SPIM}(442)^*}$	0.0574	Field measurements
Detrital Scale Factor	3.44	Field measurements
$Q$	3.6	Model Optimisation
Surface Reflectance	1.04	Typical value June – July at 12:00 at 58–59 latitude
$\mu_0$	0.89	Typical value June – July at 12:00 at 58–59 latitude
$a_w(\lambda)$	Lookup Table	<i>Pope and Fry (1997)</i>
$b_w(\lambda)$	Lookup Table	<i>Smith and Baker (1981)</i>
$b_b$ eff phyto	0.005	<i>Sathyendranath et al. (1989)</i>
$b_b$ eff water	0.5	<i>Sathyendranath et al. (1989)</i>

The detrital absorption curve is then calculated based on the predicted value of  $a_d(400)$  using Eq. (5).

$$a_d(\lambda) = a_d(400) e^{-S_d(\lambda-400)} \quad (5)$$

Finally, for the absorption of pure water ( $a_w$ ) we used the data of *Pope and Fry (1997)* and these data were contained in the model as a lookup table.

Total backscattering ( $b_b(\lambda)$ ), is related to three separate components: water, Chl and SPIM.

$$b_b(\lambda) = b_{bw}(\lambda) + b_{bph}(\lambda) + b_{b\text{SPIM}}(\lambda) \quad (6)$$

The backscattering due to phytoplankton in Eq. (6) is calculated according to *Dekker (1993)* using an equation which calculates phytoplankton related scattering at 550 nm.

$$b_{ph}(550) = 0.12Chl \quad (7)$$

The attenuation coefficient of the phytoplankton at 550 nm ( $c_{ph}(550)$ ) can then also be calculated as the sum of the  $b_{ph}(550)$  and  $a_{ph}(550)$  (obtained from Eqs. (2)–(3)). In order to predict the spectral variation in phytoplankton derived scattering, we assume that  $c_{ph}(550)$  is constant with wavelength, which allows  $b_{ph}(\lambda)$  to be calculated as

$$b_{ph}(\lambda) = c_{ph}(550) - a_{ph}(\lambda) \quad (8)$$

The assumption of a constant phytoplankton attenuation and therefore, an inverse relationship between  $a_{ph}$  and  $b_{ph}$  is of course a simplification. However, a number of studies (*Bricaud et al.* 1983; *Davis-Colley et al.*, 1986; *Bricaud et al.*, 1988) do support this formulation finding  $a_{ph}$  and  $b_{ph}$  to vary in an inverse manner and  $c_{ph}$  to be relatively constant with wavelength. Finally, the phytoplankton derived backscattering ( $b_{bph}$ ) is considered to be 0.5 percent (bb eff phyto in Fig. 1) of the total phytoplankton derived scattering (*Sathyendranath et al.*, 1989).

Given an estimate of  $b_{bph}$  (Eqs. (7)–(8)) and a knowledge of the scattering coefficients of pure water ( $b_w$ ) (*Smith and Baker*, 1981), it is possible to estimate  $b_{bSPIM}$  from total backscattering data ( $b_b$ ) measured in the field using an *in situ* sensor (Hydroscat 6 see below). Assuming that the backscattering efficiency of pure water is 50% (*Sathyendranath et al.*, 1989),  $b_{bSPIM}$  was calculated according to Equation (9) for the 6 wavelengths measured by the Hydroscat 6 using field data collected from Lake Mälaren during 1997.

$$b_{bSPIM}(\lambda) = b_b(\lambda) - b_{bph}(\lambda) - 0.5 b_w(\lambda) \quad (9)$$

A power function (*Jupp et al.*, 1994; *Gallie and Murtha*, 1992) was defined which allowed a spectral backscattering spectra to be predicted from the value of  $b_{bSPIM}(442)$ , the Hydroscat 6 measurement with the shortest wavelength.

$$b_{bSPIM}(\lambda) = b_{bSPIM}(442) \lambda^{-Bb_b/442^{-Bb_b}} \quad (10)$$

The coefficient  $Bb_b$  was determined by fitting  $b_{bSPIM}(\lambda)$  values in the Hydroscat 6 wavebands to Equation (10).

The backscattering at 442 nm ( $b_{bSPIM}(442)$ ) was related to the concentration of SPIM by regression analysis

$$b_{bSPIM}(442) = Conc\ SPIM\ b_{bSPIM}^*(442) \quad (11)$$

The derived slope of the relationship is the SPIM-specific backscattering at 442 nm.

Thus, SPIM related backscattering is calculated from the SPIM concentrations using Eqs. (10)–(11) and phytoplankton related backscattering is calculated from the Chl concentration using Eqs. (7)–(8).

Irradiance reflectance below the waters surface ( $E_u/E_d 0-$ ) is calculated according to the equation suggested by *Kirk* (1984)

$$E_u/E_d(\lambda) = (0.975 - 0.629\mu_0)b_b(\lambda)/(a(\lambda) + b_b(\lambda)) \quad (12)$$

Where  $\mu_0$  is the cosine of the solar zenith angle under the waters surface. Radiance reflectance ( $L_u/E_d 0-$ ) is calculated from irradiance reflectance by dividing the later by the so called Q factor which is a wavelength independent estimate of the ratio of  $E_u$  to  $L_u$

$$L_u/E_d(\lambda, 0-) = (E_u/E_d(\lambda, 0-))/Q \quad (13)$$

*Kirk* (1994) suggests that the values of Q range between 3.14 and 5. We estimated Q by running our model with site specific parameter values and concentrations from Lake Mälaren in 1997 and optimising Q so that the simulated values of radiance reflectance best matched measured radiance reflectance data between 500–700 nm (*Pierson and Strömbeck*, 2001). The average Q value obtained was 3.606 and this was used as a fixed value for all subsequent model runs. To transfer the subsurface radiance reflectance through the surface it is necessary to account for changes in the angular distribution of the upwelling radiance which results from differences in the refractive index of water vs. air.

$$L_w 0+ = \frac{L_u 0-}{\left[\eta_w^2 / (1 - r^\circ)\right]} = \frac{L_u 0-}{1.815} \quad (14)$$

where  $L_w 0+$  is the water leaving radiance just above the surface,  $\eta_w$  is the refraction index of water (1.333) and  $r^\circ$  the frenzel coefficient for 0 degree angle of incidence which is equal to 0.021. Based on the above the ratio of water leaving radiance to downwelling radiance above the surface (model output) was calculated as

$$L_w / E_d 0+ = \frac{L_u 0- / 1.815}{1.04 E_d 0-} \quad (15)$$

Where the factor 1.815 accounts for the radiance focusing through the waters surface and where 1.04 accounts for the fact that on approximately 4% of the downwelling irradiance is reflected from the water surface.

## 2.2 Model parameter values

The model parameter values used in all model runs in this paper and the sources from which they are derived are given in Table 1. The first 8 parameter values were derived from our field work on Lake Mälaren during August and September of 1997, while the remaining are taken from published sources. The field data were collected when the water column was well mixed and vertical variations in the IOPs were small.

Variations in vertical stratification therefore, was not a significant source of variability in our measurements. The details of the field and laboratory measurements and the data processing needed to ultimately derive these parameters are given briefly below, but are described in detail by *Strömbeck and Pierson (2001)*. All the parameter values listed in Table 1 are mean values of all the measurements carried out during the 1997 field season, and these measurements were made over a large range of IOPs and optically active concentrations (Table 2) which are characteristic of Lake Mälaren (see Fig. 3 below).

Table 2. Range in the optically active concentrations and the inherent optical properties measured in Lake Mälaren during the fall of 1997.

	Maximum	Minimum	Number of Samples
<b><i>Optically Active Concentrations</i></b>			
Chl (mg l <sup>-1</sup> )	33.2	4.4	63
SPIM (mg l <sup>-1</sup> )	9.1	0.2	62
<b><i>Inherent Optical Properties</i></b>			
aph(400) (m <sup>-1</sup> )	0.425	0.015	53
ad (400) (m <sup>-1</sup> )	0.90	0.15	57
ay (400) (m <sup>-1</sup> )	5.9	2.0	63
bb(442) (m <sup>-1</sup> )	0.659	0.022	57

The spectral absorption coefficients of phytoplankton ( $a_{ph}(\lambda)$ ) and detrital material ( $a_d(\lambda)$ ) were determined from particulate material collected on Whatman GF/F filters following the methods of *Cleveland and Weideman (1993)* and *Tassan and Ferrari (1995)*. For each measured  $a_{ph}^*$  spectrum ( $n=53$ ), regressions (analogous to *Bricaud et al., 1995*) were used to define power functions between  $a_{ph}^*(\lambda)$  and the Chl concentration. The spectral coefficients  $A(\lambda)$  and  $B(\lambda)$  derived in this manner were contained in our model in lookup tables. The slope factor of the  $a_d$  absorption curve ( $S_d$ ) was calculated for each  $a_d$  spectra by linear regression between wavelength and the natural logarithm of  $a_d(\lambda)$  in the wavelength interval between 400–550 nm.

The spectral absorption of dissolved yellow substances ( $a_y(\lambda)$ ) was spectrophotometrically measured in a 10 cm cuvette using water which passed through GF/F filters. The slope factor of the  $a_y$  absorption curve ( $S_y$ ) was calculated by regression analysis as described for  $S_d$  above.

The backscattering coefficient ( $b_b$ ) was measured using a HOBI Labs HydroScat-6 (*Maffione and Dana, 1997*) backscattering sensor which measured in six different narrow wavelength bands centered at: 442, 470, 510, 589, 620 and 671 nm. The measurements were corrected using an independent attenuation correction developed for Swedish lake waters (*Strömbeck, 1998*).

### 2.3 Analysis of historical optically active concentration data

Given a functioning model (Fig. 1, Eqs. (1)–(15)), and the necessary parameter values (Table 1) it is then possible to simulate variations in radiance reflectance for a given water body based on a knowledge of the variations in the optically active concentrations which drive the model. Chl and  $a_y(420)$  are measured as part of the routine monitoring of Lakes Mälaren, Vättern and Vänern, and these measurement can be directly input to the model (Fig. 1). Unfortunately, no routine measurements of SPIM concentration are made, but unfiltered absorption measurements at 420 nm are available. We therefore, used the difference between the unfiltered and filtered absorption at 420 nm to provide a rough estimate of SPIM concentration. To do this we assume that for unfiltered water, measurements made by a laboratory spectrophotometer are similar to those of a beam transmissometer i.e. the spectrophotometer measures the total attenuation of light ( $c$ ) which is due to both absorption and scattering. Total attenuation can be apportioned into sources associated with SPIM ( $c_{\text{SPIM}}$ ), phytoplankton ( $c_{\text{ph}}$ ) and dissolved yellow substances ( $c_y$ ). The absorption of water does not need to be accounted for since presumably the spectrophotometric measurements were referenced against a distilled water blank.

$$c(420) = c_{\text{SPIM}}(420) + c_{\text{ph}}(420) + c_y(420) \quad (16)$$

Since there is virtually no scattering associated with the dissolved material  $c_y(420)$  equals the measured dissolved absorption at 420 nm ( $a_y(420)$ ). Furthermore, following the reasoning discussed earlier  $c_{\text{ph}}(550)$  can be calculated according to Equations (2), (3) and (7), and  $c_{\text{ph}}(550)$  is assumed not to vary with wavelength so that  $c_{\text{ph}}(550)$  equals  $c_{\text{ph}}(420)$ . Then from the total attenuation measured in the spectrophotometer we estimate the attenuation coefficient due to SPIM.

$$c_{\text{SPIM}}(420) = c(420) - c_{\text{ph}}(550) - a_y(420) \quad (17)$$

It was further assumed that the majority of SPIM derived attenuation was due to scattering so that SPIM concentrations were then back calculated from the SPIM derived scattering ( $b_{\text{SPIM}}(420) = c_{\text{SPIM}}(420)$ ) based on an iterative process. The particle scattering efficiency was calculated according to *van de Hulst* (1957)

$$Q_{\text{scat}} = 2 - \frac{4}{\rho} \sin \rho + \frac{4}{\rho^2} (1 - \cos \rho) \quad (18)$$

and  $\rho$  was calculated as

$$\rho = \frac{4\pi r}{(\lambda / n_w)} (n_p - 1) \quad (19)$$

$Q_{\text{scat}}$  is the scattering cross section of a particle divided by its geometrical cross sectional area (*Spinrad*, 1986 and *Kirk*, 1994),  $r$  is the particle radius and  $\eta_p$  and  $\eta_w$  are the

refractive indexes of the inorganic particles and water respectively. A  $\eta_p$  value of 1.17 was used following *Kirk* (1994). Inorganic scattering for a given size particle is the product of this efficiency factor, the particle cross sectional area, and the total number of particles of that size.

The scattering for the entire population of particles in the sample was calculated based on the particle size distribution suggested by *Risovic* (1993)

$$\text{PartNum} = C r^2 e^{-\beta r^\gamma} \quad (20)$$

PartNum is the total particle number of a given radius and  $\beta$ ,  $\gamma$  and  $C$  are constants in the equation of the gamma distribution. Following *Risovic* (1993),  $\beta$  was assumed to have a value of  $-52$  and  $\gamma$  was given a value of  $0.157$ . Twenty size class groups were used in the particle size and scattering calculations. The size groups ranged from  $0.1 \mu\text{m}$  to  $20 \mu\text{m}$  with a  $1 \mu\text{m}$  step. The constant  $C$  was adjusted so that the total scattering calculated using the above distribution function in conjunction with Equations (18) and (19) is equal to the estimate of  $b_{\text{SPIM}}(420)$ . Knowing  $C$  the particle numbers in each size class are then calculated using Equation (20) and these are converted to a weight assuming an inorganic density of  $2.6 \text{ g cm}^{-3}$  and that the particles are spherical.

A weakness associated with the above method for estimating SPIM lies in assumption that a laboratory spectrophotometer measures  $c(420)$ . In reality, spectrophotometers are not designed to measure attenuation, and as a result some forward scattered light is detected, which consequently leads to an underestimation of  $c$  and SPIM (Eq. (17)). To correct for such an underestimation of  $c(420)$  we made use of an independent data set from two basins of Lake Mälaren (Ekoln and Galten) where the chlorophyll concentration, and filtered and unfiltered absorption at  $420 \text{ nm}$  were measured as in the Swedish Environmental protection agency database, and where SPIM was also measured by gravimetric analysis. A correction factor was added to the model which allowed the magnitude of  $c(420)$  to be adjusted, and this factor was optimised to best match the measured and simulated SPIM concentrations. Increasing  $c(420)$  by a factor of  $1.29$  led to a good match between simulated and measured SPIM concentrations (Fig. 2). However, as can be seen from the scatter in the upper portion of Fig. 2, these estimates contain errors which are associated with a number of the assumptions in the model such as a consistent particle size distribution, particle shape, particle refractive index, etc. Never the less, this method does calculate SPIM concentration in a realistic and consistent manner that makes the best use of available historical data. To illustrate this the SPIM distributions for the Ekoln and Galten basins were estimated from the filtered and unfiltered absorption at  $420 \text{ nm}$  and chlorophyll concentrations using both the long term historical data set and the shorter independent data set. The frequency distributions derived from both data sets are quite similar (Fig. 2). The greatest difference between the frequency distributions is that the longer (larger) data set measures a greater frequency of high concentrations, which is of course to be expected.

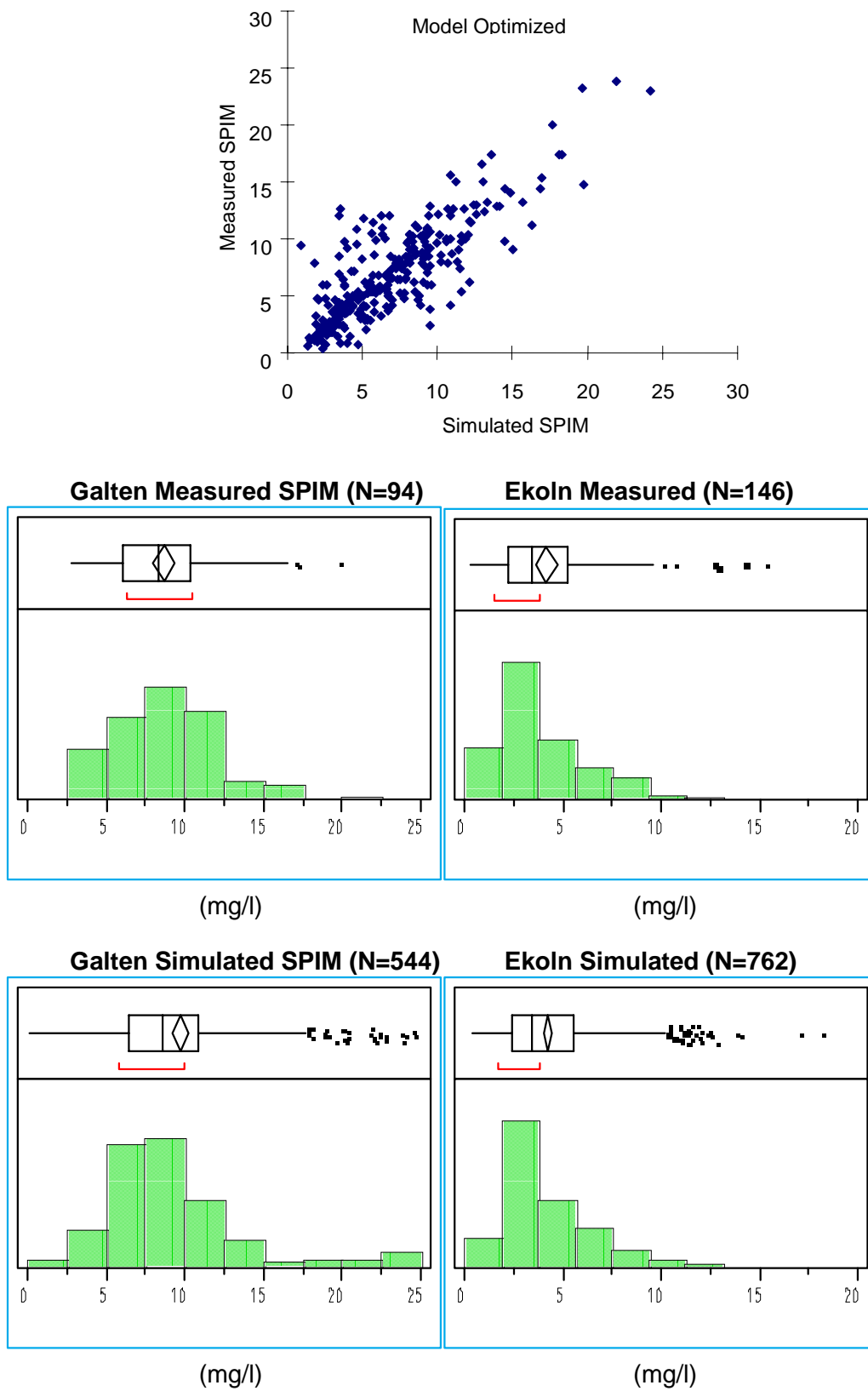


Fig. 2. Relationship between simulated SPIM concentrations (Eqs. (16)–(20)) and SPIM concentrations measured by gravimetric analysis using data from two basins in Lake Mälaren. (Top) This plot is obtained after optimising the value of  $c(420)$  as described in the text. Bottom portion of this figure shows the simulated frequency distributions of SPIM for the two sites based on two independent data sets.

#### 2.4 *Method of sensitivity analysis*

To simulate typical variations in water leaving radiance reflectance ( $L_w/E_d 0+$ ), 500 separate simulations were made for each lake. For each simulation a new value of each of the optically active concentrations driving the model (Fig. 1) was randomly chosen from a gamma distribution which was found to fit the concentration distributions of the historical data from each lake (Fig. 3). An example of the variations in radiance reflectance simulated for Lake Mälaren is given in Fig. 4. One pitfall of the simulation method described above is that there will be a tendency to overestimate the variability in radiance reflectance if the optically active substances are correlated. Correlations between the optically active substances were weak in all lakes. It therefore, seems justified to consider the concentrations independent of each other in these simulations.

The synthetic data sets from each lake of the optically active substances and the associated radiance reflectance spectra were analysed in order to discover possible band ratios algorithms which could be used to predict the levels of the optically active substances. First, a high resolution analysis calculated the regression coefficients ( $r^2$ ) between all possible 10 nm band ratios (i.e. 405/415, 405/425 .... 735/745) and the concentrations of each of the optically active substances. Secondly, radiance reflectance in the bands of the MERIS sensor (*Brezy and Rast, 1999*) were estimated, and optimal algorithms based on these bands were evaluated.

### 3. *Results and discussion*

#### 3.1 *Historical data*

There is an extensive set of measurements, collected by the Swedish Environmental Protection Agency, from each lake, (<http://www.ma.slu.se>). Measurements began between 1966–1973 and are continuing today. Between 11 and 4 sampling sites are visited on each lake and samples are usually collected 7 times per year. As a result, a sample size of approximately 2200, 1500 and 400 was available for lakes Mälaren, Vänern, and Vättern respectively, although the actual number varies somewhat with the parameter in question. This unusually extensive data set provides the opportunity to realistically simulate variations in radiance reflectance over wide and well characterised variations in water quality.

In Fig. 3 the frequency distributions of the optically active substances which were measured in each lake and those which were produced in the synthetic data sets generated by the sensitivity simulations are shown. None of the optically active substances from any of the Lakes were normally distributed, but all fit well to a gamma distribution. It can be seen from these data that there is a good correspondence between the measured distributions of optically active substances in each lake and those simulated based on gamma distributions fit to the measured data. Both the magnitude and shape of

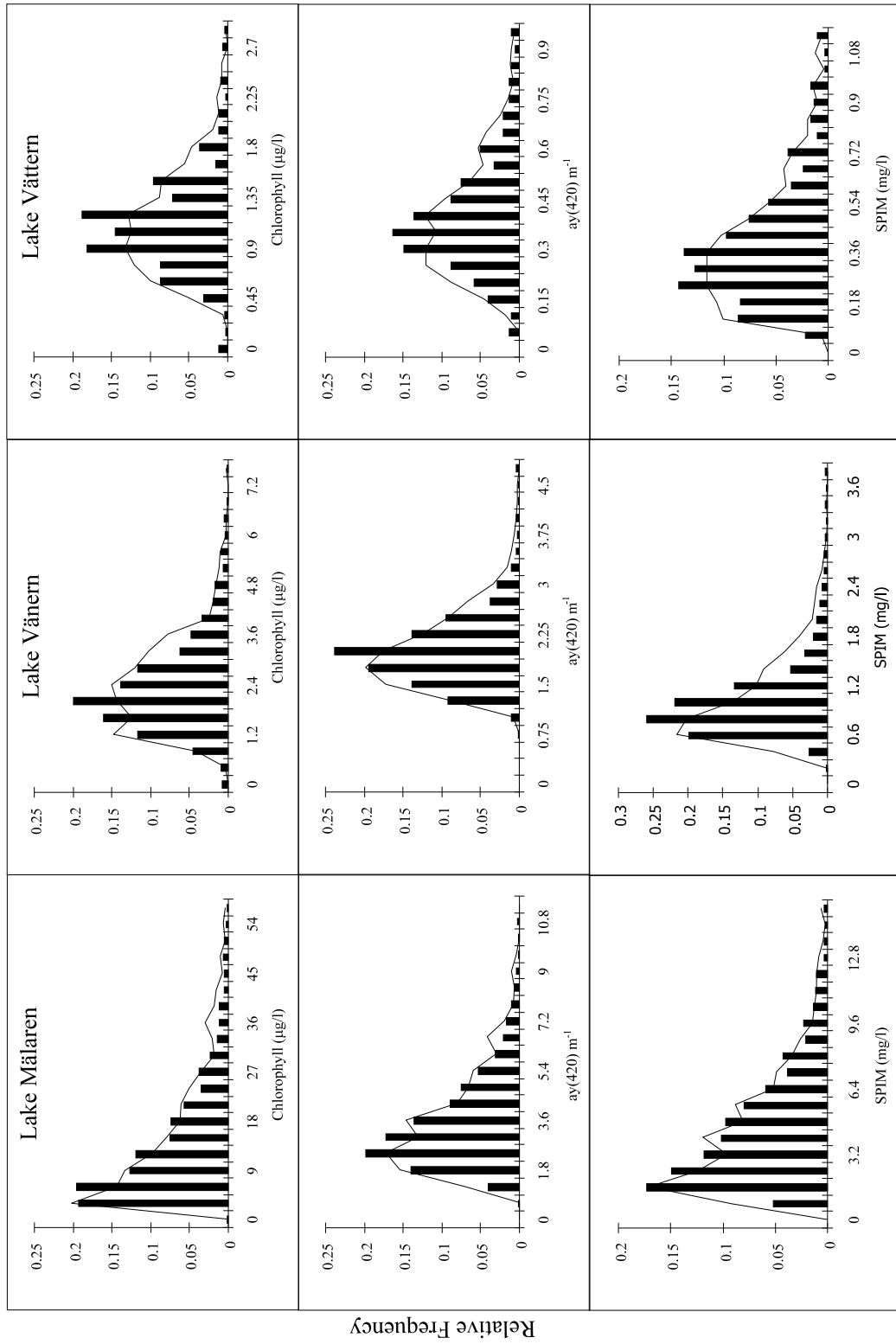


Fig. 3. Frequency distributions of the optically active substances in each Swedish great lake. The solid bars are based on the long term data set measured in each lake. The line is the distribution obtained from the 500 Monte Carlo simulations runs. Relative frequency is the number of samples in any given category divided by the total number of samples in the data set.

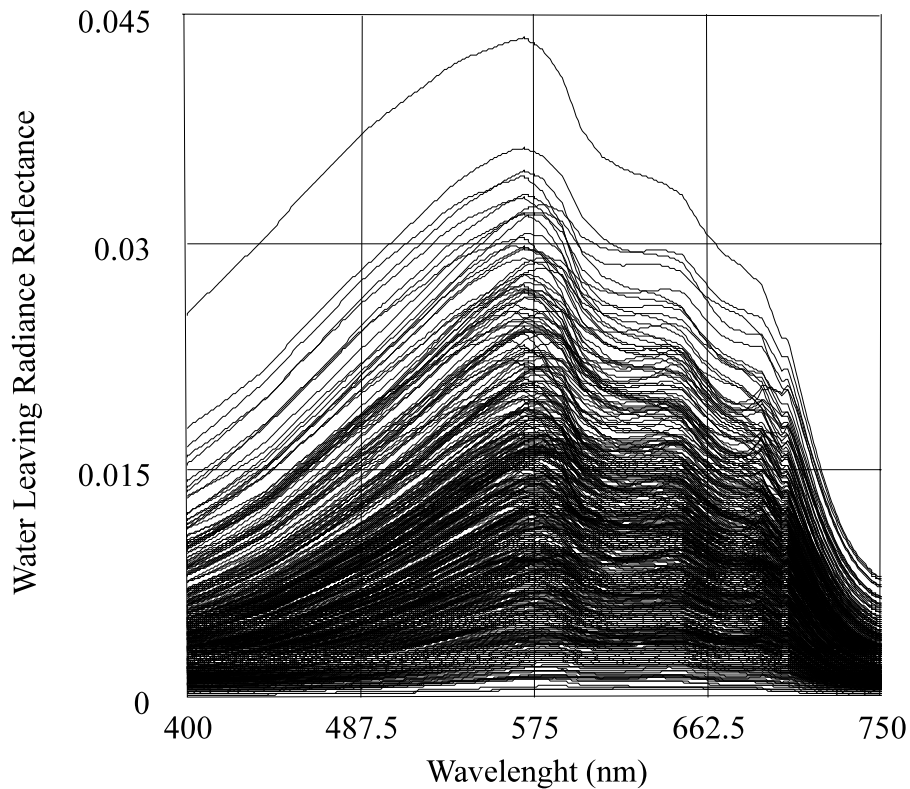


Fig. 4. The 500 spectra of radiance reflectance simulated for Lake Mälaren. The optically active substances associated with each spectra were chosen from the distributions show in Fig. 3.

the measured distributions are reproduced in the synthetic data sets. This suggests that the variability in radiance reflectance estimated from the simulations (e.g. Fig. 4) will be representative of the variability that would be measured from the lakes over the range in water quality normally occurring in each lake.

There are obvious water quality differences between the lakes. The concentrations of all of the optically active substances are greatest and most variable in Lake Mälaren. There is a strong gradient in water quality in this lake (Pierson, 1998; Wallin *et al.*, 2000) since the greatest hydrologic inputs occur in the shallow western end. As a result there are greater levels of yellow substances, nutrients and chlorophyll, and the shallow depth also leads to greater sediment resuspension and SPIM concentrations. To the east the lake deepens and the hydrologic retention time increases significantly for the deeper basins. In these deeper basins the concentrations of all optically active substances decreases. Vättern is deeper, has a longer hydrologic retention time, and a lower rate of external nutrient loading. As a result, the lake has lower concentrations of all of the optically active substances which influence estimates of radiance reflectance. However, the ratios of the optically active substances are quite similar to Mälaren (Fig. 5), especially in the case of the ratios of Chl to  $a_y(420)$  with the ratios for Mälaren and Vättern being 3.09 and 3.13 respectively. The magnitude and range in variability in Lake Vänern's optically active substances lies in between Mälaren and Vättern (Fig. 3). The lake is larger and more complex than Vättern, and as a result there is a greater variability in the optically active substances. The ratio of Chl to  $a_y(420)$  in this lake is signifi-

cantly different from the other two lakes with much greater levels of yellow substance per unit Chl (Fig. 5).

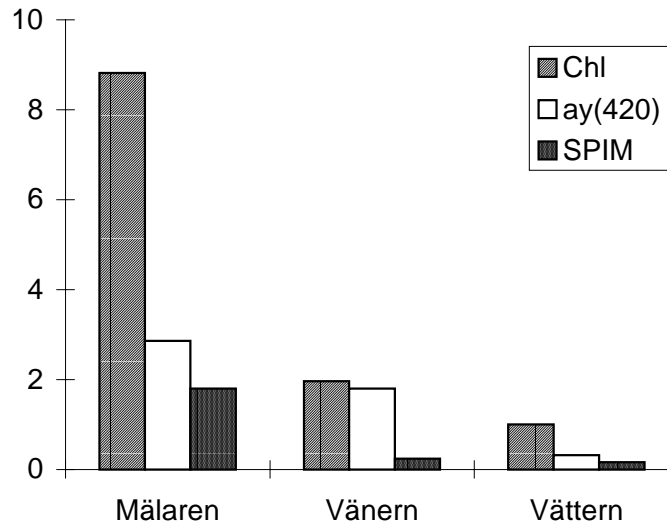


Fig. 5. The mean values of the optically active substances in each Lake. In lake Vänern chlorophyll and yellow substance are of a similar magnitude, while in the other lakes the magnitude of chlorophyll is approximately three times as great as yellow substances. Chlorophyll is in units of  $\mu\text{g l}^{-1}$ , SPIM is in  $\text{mg l}^{-1}$  and  $a_y(420)$  is in  $\text{m}^{-1}$ .

The consequent effects of these differences in the optically active substances is illustrated by Fig. 6 where radiance reflectance is simulated using the mean concentration values in Fig. 5. Mälaren shows the highest reflectance over the entire simulated spectra, which is a result of the high SPIM concentrations in this lake. These result in greater levels of backscattering and thereby greater reflectance, even though the higher concentrations of the Chl and yellow substances will reduce reflectance due to their effects on absorption. The affects of SPIM on the reflectance spectra are clear at wavelengths greater than 600 nm where the relative differences in reflection are similar to the differences in SPIM (Fig. 5). The mean yellow substance absorption is similar in Mälaren and Vänern, but much less in Vättern. These differences are apparent in the shape of the reflection spectra between 400–550 nm. The shape of the Vättern reflectance spectra is clearly more influenced by Chl than in the other two lakes where yellow substance absorption is the dominate factor influencing the shape of the reflectance spectra in this region. The lower reflectance simulated in the blue-green wavelengths for Vänern are the result of the higher yellow substance concentrations in this lake, and relatively low SPIM concentrations. The broadest absorption band of Chl is in the 400–550 nm range, and ocean remote sensing algorithms make use of reflectance ratios based on bands in this spectral range. For example, the SeaWiFS OC2v2 chlorophyll algorithm (*O'Reilly et al.*, 1998) makes use of the 490 nm and 555 nm SeaWiFS chan-

nels. As in other freshwater and coastal environments, these types of algorithms will not be successful when applied to the Swedish great lakes: The 490 nm reflectance values in lakes Vättern and Mälaren differ by only 28% despite eight fold differences in Chl concentration.

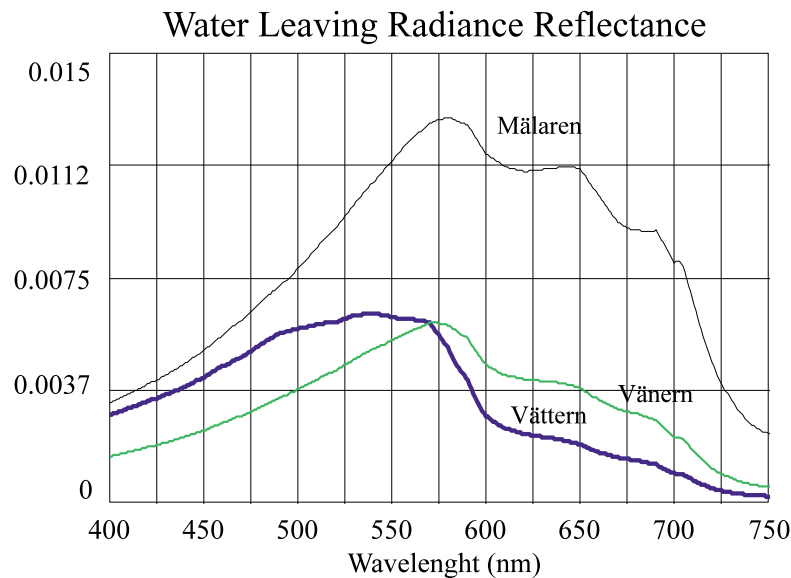


Fig. 6. Radiance reflectance spectra simulated for each of the Swedish great lakes when the optically active substances used to drive the model were set at the mean values shown in Fig. 5.

### 3.2 General algorithm development

Examination of the synthetic data set shows SPIM concentrations to be strongly related to the reflectance measured at wavelengths greater than 550 nm. The best relationships are those with wavelengths greater than 680 nm since above this wavelength absorption is almost entirely due to water (which does not change) and therefore, variations in reflection are predominately the result of variations in backscattering (Eq. (12)) which in turn are related to the SPIM concentration (Eqs. (10)–(11)). Consequently in all lakes strong correlations ( $r^2 > 0.9$ ) were found between SPIM and radiance reflectance at a wavelengths greater than 680 nm., and as a result optimal SPIM algorithms can be based on a linear regression using reflectance values at wavelengths greater than 680 nm as the independent variable. At 550 nm the  $R_r$  vs. SPIM relationship is more noisy since the absorption of the other optically active substances also has an affect on the simulated reflection, and these of course, vary between simulations. Never the less, all lakes showed a strong correlation between  $R_r$  (550) and SPIM ( $r^2$  exceeded 0.77 in all lakes). This can be of significance since maximum reflectance occurs between 550–580 nm (Fig. 6). Reflectance values in this spectral region can therefore, be used to predict SPIM even when the red reflectance levels are low, and consequently prediction of SPIM should successful under most probable conditions.

In the case of Chl and  $a_y(420)$  direct relationships between these substances and a single wave band were not strong. Instead, band ratio algorithms were investigated by estimating the correlation coefficients between these optically active concentrations and all possible 10 nm band ratios estimated from the reflectance spectra in the synthetic data sets. For example, the correlation was estimated between Chl and the 405 nm/415 nm ratio using the 500 simulated cases in each lake's data set. This calculation was then followed by the 405 nm/425 nm ratio and so on until all 1225 possible correlation coefficients had been calculated. The results of these calculations are presented graphically as a shaded surface in Fig. 7 where the correlation coefficient for any band1 (y-axis) / band 2 (x-axis) ratio can be seen.

These results suggest that concentrations of Chl will be best estimated using a ratio of a band greater than 700 nm (band 1) to a band between 660–680 nm (band 2). This band ratio algorithm normalises changes in reflection brought about by changes in Chl related absorption between 660–680 nm by backscattering related changes in reflection detected at wavelengths greater than 700 nm. Given that reflectance is directly proportional to backscattering and inversely proportional to absorption (Eq. (12)), the ratio of the wave band effected most by backscattering (> 700 nm) to that influenced most by Chl absorption (660–680 nm) will yield a positive relationship with Chl. It is significant that this simple band ratio algorithm performs well in all three lakes which cover a wide range of optically active substances (Fig. 3). It is also of significance that band ratios using the blue chlorophyll absorption band were useless due to interference from yellow substance absorption. Comparison of the chlorophyll band ratio results (Fig. 7) with the mean concentration data (Fig. 5), provides information on the influence of the other optically active substances on the success of chlorophyll band ratio algorithms. Good results are obtained in Mälaren and Vättern which have similar ratios of Chl to  $a_y(420)$ . In these lakes the concentration of Chl is sufficiently greater than that of yellow substances, so that the yellow substances do not significantly influence the absorption in the 660–680 nm spectral region. This is not the case in Vänern. Here the relative concentration of yellow substances to Chl is 3 time greater than in the other two lakes, and as a result variations in yellow substances can add significant variations to the 660–680 nm absorption, and in doing so add noise to the chlorophyll band ratio regression.

Band ratio algorithms to estimate the concentration yellow substances ( $a_y 420$ ) are also examined in Fig. 7, where it can be seen that the best algorithms are based on a ratio of a reference band greater than 600 nm (band 1) to a band affected by yellow substance absorption between 400–580 nm. These algorithms work for much the same reason as Chl algorithms described above: Changes in reflection brought about by changes in yellow substance related absorption are normalised by non-yellow substance related changes in reflection detected at wavelengths greater than 600 nm.

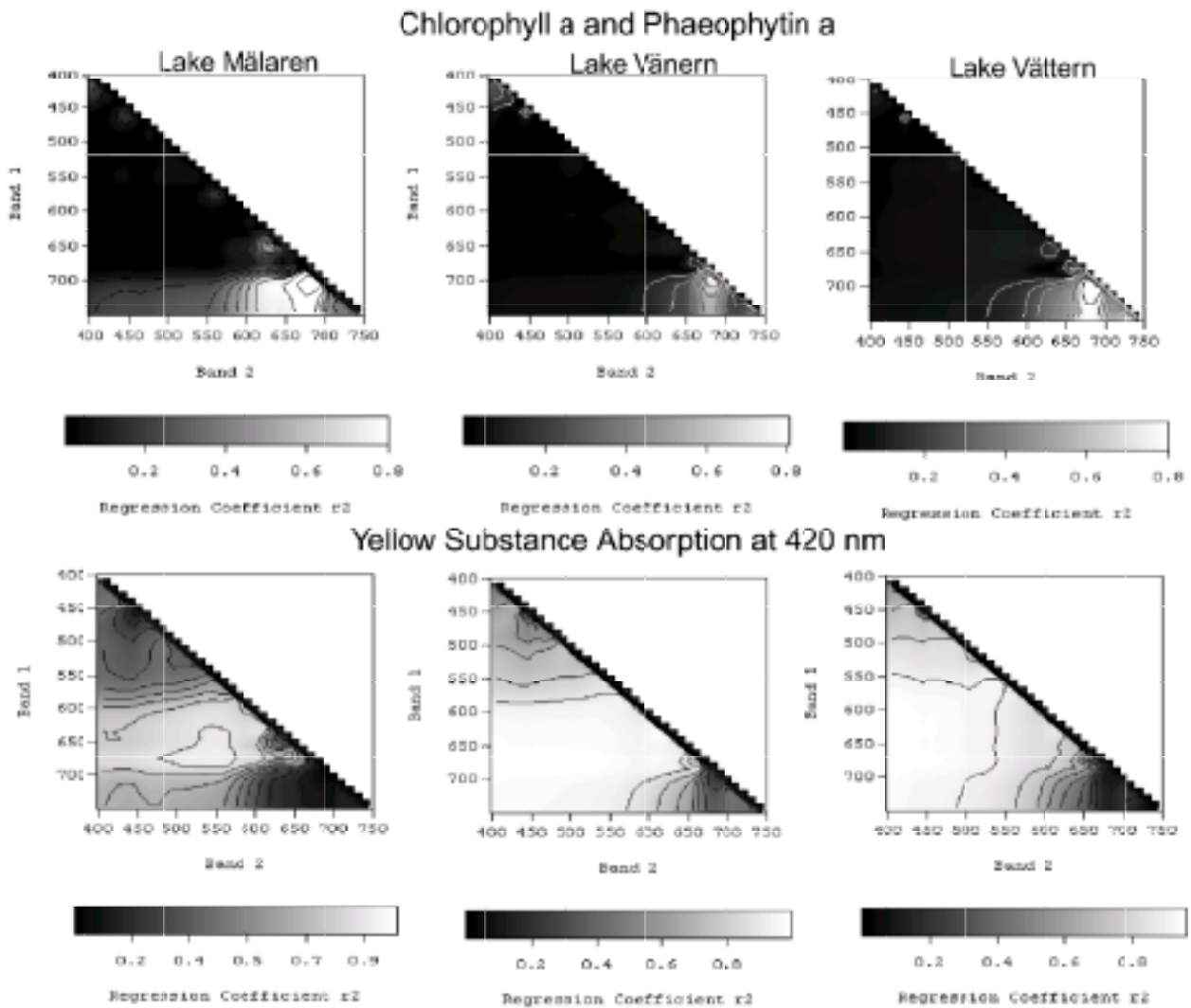


Fig. 7. Surface plots of the correlation coefficients ( $r^2$ ) for all possible 10 nm band ratios vs. the concentration of Chl or  $a_y(420)$ . The correlation coefficient for the band1/band2 is read as the shadows of point (y,x) where y = band 1 and x = band 2. These correlations were based on the synthetic data sets of 500 radiance reflectance spectra and 500 associated sets of optically active concentrations for each lake.

The importance of a 600–700 nm reference band is quite obvious in the case of Lake Mälaren (Fig. 7), where phytoplankton pigment concentrations are greatest (Fig. 5) and the affect becomes progressively less in Vänern and then Vättern in proportion with their lower pigment concentrations. In Fig. 8 two of the yellow substance algorithms derived from the synthetic Mälaren data set are shown. One is normalised using a band outside the pigment absorption band (745/405) while the other is normalised using a band within the pigment absorption band (675/405). It is evident that the scatter is greater when the 405 nm reflectance is normalised by the 745 nm reflectance. Normalisation using the 660–680 nm spectral region does not simply account for variations in SPIM related backscattering, but is also related to Chl concentration and in turn on the dependence of both absorption and scattering on Chl, as parameterized in our model. In regards to the example in Fig. 8, increasing Chl will increase  $a_{ph}$  which will in turn influence  $a(405)$  independently of changes in  $a_y$ . Likewise, increases in Chl will

increase phytoplankton induced backscattering ( $b_{\text{bph}}$ ), but this increase will be inversely proportional to phytoplankton absorption (Eq. (8)). Therefore,  $b_{\text{bph}}$  induced variations in  $R_r$  675 will be less since this is an absorption peak of Chl which reduces the overall variability in  $b_{\text{bph}}$ , while at 745 nm  $b_{\text{bph}}$  related variations in  $R_r$  will be maximum since  $a_{\text{ph}}$  is minimal. It appears as though it is the effect of phytoplankton on scattering that is most important in enhancing the yellow substance algorithms normalised using the 660–680 nm band.

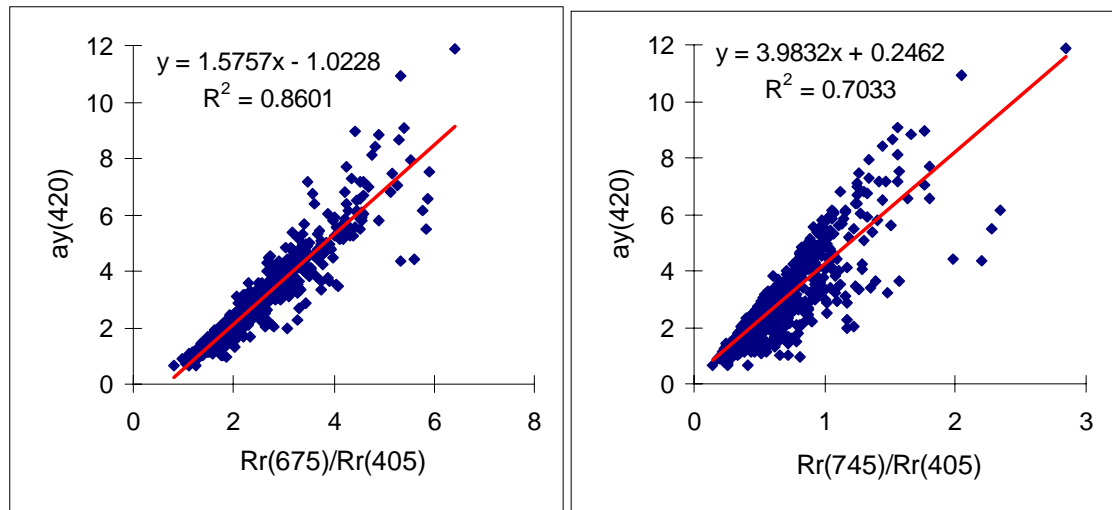


Fig. 8. Examples of yellow substance band ratio relationships from Lake Mälaren in which band 1 is in the chlorophyll absorption band between 660–680 nm, and when band 1 exceeds 700 nm. Failure to make use of the chlorophyll absorption band increases the noise in the band ratio algorithm.

Whether the dependence of yellow substance algorithms on reflectance measurements in the 660–680 nm band is real or an artifact of our parameterization of  $b_{\text{bph}}$  is at this point uncertain. Actual measurements of the spectral variability in  $b_{\text{bph}}$  are limited (Kiefer *et al.*, 1979; Bricaud *et al.*, 1983; Davis-Colley *et al.*, 1986; Bricaud *et al.*, 1988; Ahn *et al.*, 1992) making it difficult to verify  $b_{\text{bph}}$  parameterization. The equations we have used to describe spectral variation in  $b_{\text{bph}}$  is based on the assumption that  $a_{\text{ph}}$  and  $b_{\text{ph}}$  are inversely related and  $c_{\text{ph}}$  is relatively independent of wavelength. These assumptions are both physically plausible and observed in laboratory studies (Bricaud *et al.*, 1983; Davis-Colley *et al.*, 1986; Bricaud *et al.*, 1988). We are working on an analysis analogous to Fig. 7 that will be based on actual *in situ* measurements of radiance reflectance, the results of which should settle this question. But, for the time being, the results of these simulations suggest that the use of the 660–680 nm band may well lead to improved yellow substance algorithms.

### 3.3 MERIS algorithms

In addition to estimating water leaving radiance reflectance in 10 nm bands as described above we also estimated radiance reflectance in the bands of the MERIS sensor,

and based on the results in Fig. 7 we developed and tested optimal MERIS algorithms. Plots of the optimal band or band ratio vs. the concentrations of optically active substances are shown in Fig. 9. Concentrations of Chl were best predicted using the band 9 (705 nm) to band 7 (665 nm) ratio. And, as discussed above, the noise in the Chl predictions is greatest in Vänern due to the high concentrations of yellow substances relative to Chl. Estimates of yellow substance absorption ( $a_y(420)$ ) can be predicted with a high degree of certainty based on the ratio of band 7 (665 nm) / band 3 (490 nm). However, any of MERIS bands 1 (412 nm) through 5 (560 nm) can be used in the denominator of the yellow substance band ratio (Fig. 7) The 490 nm band was chosen since it was at a short enough wavelength to be strongly influenced by yellow substance absorption, but it was not in the shortest blue wavebands where atmospheric correction is particularly difficult. Prediction of SPIM could be based on a correlation against a single MERIS band and all bands above band 5 (560 nm) provided satisfactory results. In Fig. 9 the band 9 (705 nm) relationship is shown, since this band produced the best result. However, radiance reflectance in this band is quite low, and if acceptable signal to noise can not be obtained under the conditions of actual measurements, a shorter wave band could also be used.

#### 4. Conclusions

We have verified that our model can reproduce the spectral variations in radiance reflectance to a reasonable degree of accuracy by comparing simulated and measured  $R_r$  spectra at 12 sites in Lake Mälaren sampled during 1997 (Pierson and Strömbeck, 2001). Our present data are not however, extensive enough to make independent verification of the results in Fig. 7 or 9, but work is under way to process and collect *in situ* measurements of radiance reflectance which will allow an independent check of these results. Here we demonstrate the utility of a modelling approach to develop and evaluate preliminary remote sensing algorithms. The advantages of this approach is that it is rapid and easy to employ, and not dependent on extensive field measurements; and given the high spectral resolution of our model, it is possible to examine algorithms for both presently available and future sensors. In cases where there exist extensive data sets of the optically active concentrations, such as the Swedish great lakes, modelling provides the ability to simulate variations in radiance reflectance over large variations in space and time; more so than would normally be sampled by an *in situ* measurement campaign.

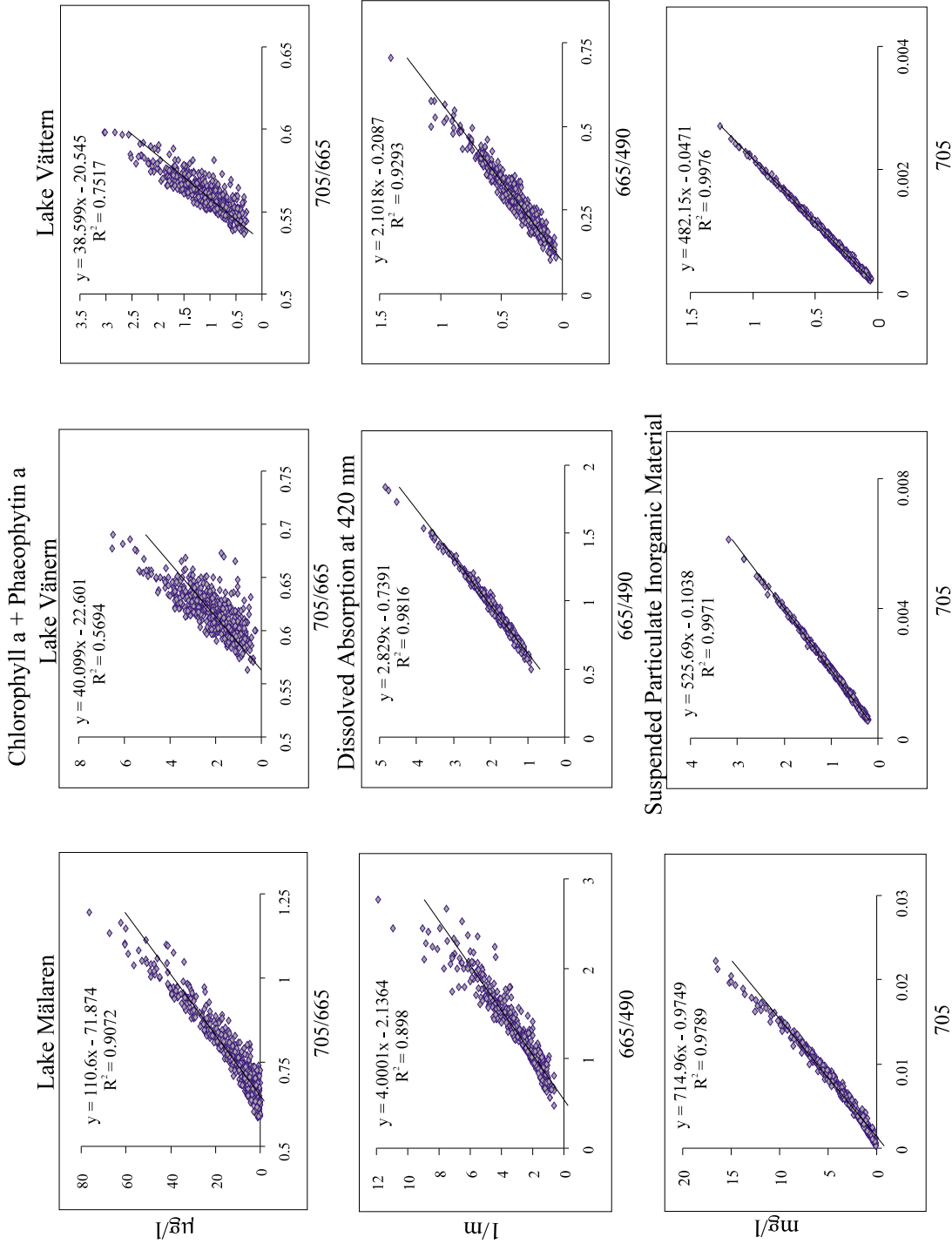


Fig. 9. Optimum MERIS algorithms to estimates the optically active substances in each Swedish great lake. These figures are based on the synthetic data set generated for each lake.

An important conclusion of this work is that the chlorophyll absorption band between 660–680 nm plays a crucial role in the success of freshwater remote sensing algorithms to predict Chl and may also be valuable for the prediction of yellow substances. Therefore, there is a need to carefully examine the accuracy of measurements, and to obtain experimental data on the processes affecting both scattering and absorption in this spectral region. For example,  $a_y$  predicted by standard algorithms (Eq. (4)) can be of the same order of magnitude as  $a_{ph}$  in the 660–680 nm band in moderate to highly colored lakes. In such a case it is critical to know if this predicted  $a_y$  absorption is real or an artifact of the algorithm predicting it. Of course the algorithms are based on field measurements, but it can be difficult to ensure that the relatively low  $a_y$  values at long wavelengths are the result of absorption and not a small amounts of residual scattering through the long (5–10 cm) path used in the spectrophotometric measurements. Correction procedures to remove scattering effects are different, and  $a_y(660-680)$  can vary significantly depending on the chosen correction. Similar problems exist in estimating  $b_b$  in the 660–680 nm region. At present parameterization of  $b_{bph}$  in this region of the spectra is quite uncertain, based largely on a theoretical relationship between spectral variations in  $a_{ph}$  and  $b_{bph}$  (e.g. *Sathyendranath*, 1989), and/or a very limited number of measurements made on laboratory cultures (*Kutser*, 1997). The Hydroscat 6 sensor provides estimates of total  $b_b$  (which must themselves be corrected) at the 620 and 671 nm wavelengths, and provides valuable information for model parameterization. Never the less, assumptions must be made about the magnitude and variability of  $b_{bph}$  in order to develop  $b_{bSPIM}$  and  $b_{bph}$  specific coefficients needed to separately model the influences of both substances on radiance reflectance (Eqs. (7)–(9)).

If these preliminary results hold after field validation, and when including the affects of atmospheric correction procedures on the predicted radiance reflectance, an important result is obtained: Prediction of the optically active substances in lakes may be accurately made using only 3 well defined wave bands. Of most importance is a band in the chlorophyll absorption peak between 660–680 nm followed by a measurement at a long wavelength ( $> 680$  nm) to estimate scattering related influences, and a measurement in the short wavelengths (400–550 nm) to estimate the influence of yellow substances on variations in radiance reflectance. In addition, one or more additional band(s) will be needed in the far red – NIR for use in atmospheric correction. A future remote sensing satellite using only these 4–5 bands could measure at higher spatial resolution than the present generation of ocean color sensors. A proper trade off using a well defined but small number of spectral bands, and a high spatial resolution is needed to monitor small or morphometrically complex water bodies.

#### *Acknowledgements*

This research was supported by the European Union Environment and Climate Program SALMON project (contract ENV4 CT96 0311), the Swedish Environmental Protection Agency, and the Swedish National Space Board (Contract 172/98). We thank

Hampus Markensten for providing the data from the Galten and Ekoln basins of Lake Mälaren, and the staff of the Erken Laboratory of Uppsala University for assistance with our laboratory work.

### References

- Ahn, Y.H., A. Bricaud and A. Morel, 1992. Light backscattering efficiency and related properties of some phytoplankters, *Deep Sea Res.*, **39**, 1835–1855.
- Arst, H., S. Mäekivi, T. Lukk and A. Herlevi, 1997. Calculating irradiance penetration into water bodies from the measured beam attenuation coefficient, *Limnol. Oceanogr.*, **42**, 379–385.
- Bezy, M. and J.L. Rast, 1999. The ESA Medium Resolution Imaging Spectrometer MERIS a review of the instrument and its mission, *Int. J. Remote Sens.*, **20(9)**, 1681–1702.
- Bricaud, A., A. Morel and L. Prieur, 1981. Absorption by dissolved organic matter in the sea (yellow substance) in the UV and visible domain, *Limnol. Oceanogr.*, **26**, 43–53.
- Bricaud, A., A. Morel and L. Prieur, 1983. Optical efficiency factors of some phytoplankters, *Limnol and Oceanogr.*, **28(5)**, 816–832.
- Bricaud, A., A.L. Bedhomme and A. Morel, 1988. Optical properties of diverse phytoplanktonic species: experimental results and theoretical interpretation, *J. Plankton Res.*, **10(5)**, 851–873.
- Bricaud, A., M. Babin, A. Morel and H. Claustre, 1995. Variability in the chlorophyll-specific absorption coefficients of natural phytoplankton: Analysis and parameterization, *J. Geophysical Res.*, **100(C7)**, 13321–13332.
- Cleveland, J.S. and A.D. Weideman, 1993. Quantifying absorption by aquatic particles: a multiple scattering correction for glass fiber filters, *Limnol. Oceanogr.*, **38(6)**, 1321–1327.
- Davies-Colley, R.J., R.D. Pridmore and J.E. Hewitt, 1986. Optical properties of some freshwater phytoplanktonic algae, *Hydrobiologia*, **133**, 165–178.
- Dekker, A.G., 1993. Detection of optical water quality parameters for eutrophic waters by high resolution remote sensing. Ph.D. Thesis, Vrije Universiteit, Amsterdam.
- Gallie, E.A. and P.A. Murtha, 1992. Specific Absorption and Backscattering Spectra for Suspended Minerals and Chlorophyll-a in Chilko Lake, British Columbia, *Remote Sensing Environment*, **39**, 103–118.
- Gordon, H R, O.B. Brown, R.H. Evans, J.W. Brown, R.C. Smith, K.S. Baker and D.K. Clark, 1988. A semianalytical radiance model of ocean color, *J. Geophys. Res.*, **93(D9)**, 10909–10924.
- van de Hulst, H.C., 1957. *Light scattering by small particles*. Wiley, New York. (Cited by Kirk 1994).

- Jupp, D.L.B., J.T.O. Kirk and G.P. Harris, 1994. Detection, identification and mapping of cyanobacteria – using remote sensing to measure the optical quality of turbid inland waters, *Australian Journal of Marine and Freshwater Research*, **45**, 801–828.
- Kiefer, D.A., R.J. Olson and W.H. Wilson, 1979. Reflectance spectroscopy of marine phytoplankton. Part 1. Optical properties as related to age and growth rate, *Limnol. Oceanogr.*, **24(4)**, 664–672.
- Kirk, J.T.O., 1984. Dependence of relationship between inherent and apparent optical properties of water on solar altitude, *Limnol. Oceanogr.*, **29**, 350–356.
- Kirk, J.T.O., 1994. *Light and Photosynthesis in Aquatic Ecosystems*. Cambridge University Press, New York. 509 pp.
- Kutser, T., 1997. Estimation of water quality in turbid inland and coastal waters by passive optical remote sensing, *Dissertationes Geophysicales Universitas Tartuensis*, **Vol. 8**, pp. 161, Tartu, Estonia.
- Lindell, T., D.C. Pierson, G. Premazzi and E. Zilioli, (Eds.), 1999. Manual for Monitoring European Lakes Using Remote Sensing Techniques. Office for Official Publications of the European Communities, Luxembourg. ISBN 92–828–5390–X 161 pp.
- Maffione, R.A. and D.R. Dana, 1997. Instruments and methods for measuring the backward-scattering coefficient of ocean waters, *Applied Optics*, **36(24)**, 6057–6067.
- Morel, A., 1988. Optical modeling of the upper ocean in relation to its biogenous matter content (case I waters), *J. Geophys. Res.*, **93(C9)**, 10749–10768.
- Nelson, J.R. and S. Guarda, 1995. Particulate and dissolved absorption on the continental shelf of the south-eastern United States, *J. Geophys. Res.*, **100**, 8715–8732.
- O'Reilly, J.E., S. Maritorena, B.G. Mitchell, D.A. Siegel, K.L. Carder, S.A. Garver, M. Kahru and C. McClain, 1998. Ocean color chlorophyll algorithms for SeaWiFS, *J. Geophys. Res.*, **103(C11)**, 24,937–24,953.
- Pierson, D.C., 1998. Measurement and modeling of radiance reflectance in Swedish waters, *First EARSeL workshop on Imaging Spectroscopy*, pp. 207–214. Zurich, Switzerland.
- Pierson, D.C. and N. Strömbeck, 2001. Estimation of radiance reflectance and the concentrations of optically active substances in Lake Mälaren, Sweden based on direct and inverse solutions of a simple model, *Science of the Total Environment*, (in press).
- Pope, M. and E.S. Fry, 1997. Absorption spectrum (380–700 nm) of pure water. II Integrating cavity measurements, *Applied optics*, **36(33)**, 8710–8723.
- Risovic, D. 1993. Two-component model of sea particle size distribution, *Deep-Sea-Res.-I-Oceanogr.-Res. Pap.* **40(7)**, 1459–1473.

- Sathyendranath, S., L. Prieur and A. Morel, 1989. A three-component model of ocean colour and its application to remote sensing of phytoplankton pigments in coastal waters, *Int. J. Remote Sens.*, **10**, 1373–1394.
- Smith, R.C. and K.S. Baker, 1981. Optical properties of the clearest natural waters (200–800 nm), *Appl. Optics*, **20**, 177–184.
- Spinrad, R.W., 1986. A calibration diagram of specific beam attenuation, *J. Geophys. Res.*, **91(C6)**, 7761–7764.
- Strömbeck, N., 1998. Attenuation based correction of spectral backscattering in Lake Mälaren, Central Sweden, *First EARSeL workshop on Imaging Spectroscopy*, pp. 221–228, Zurich, Switzerland
- Strömbeck, N. and D.C. Pierson, 2001. The effects of variability in the inherent optical properties on estimations of chlorophyll *a* by remote sensing in Swedish freshwaters, *Science of the Total Environment*, (in press).
- Tassan, S. and G.M. Ferrari, 1995. An alternative approach to absorption measurements of aquatic particles retained on filters, *Limnol. Oceanogr.*, **40(8)**, 1358–1368.
- Wallin, M. (Ed.), 2000. Mälaren miljötillstånd och utveckling 1965–1998. *Report of Mälarens vattenvårdsförbund*, Länsstyrelsen, Västmanlands län, Västerås, Sweden, (in Swedish).

*Appendix I – List of abbreviations*

$a(\lambda)$	total absorption coefficient ( $\text{m}^{-1}$ )
$a_d(\lambda)$	detrital absorption coefficient ( $\text{m}^{-1}$ )
$a_{ph}(\lambda)$	phytoplankton absorption coefficient ( $\text{m}^{-1}$ )
$a_{ph}^*(\lambda)$	chlorophyll specific absorption coefficient ( $\text{m}^2 \text{mg}^{-1}$ )
$a_w(\lambda)$	absorption coefficient of pure water ( $\text{m}^{-1}$ )
$a_y(\lambda)$	yellow substance absorption coefficient ( $\text{m}^{-1}$ )
$b_b(\lambda)$	total backscattering coefficient ( $\text{m}^{-1}$ )
$B_{bb}$	exponent for SPIM backscattering
$b_{bph}(\lambda)$	phytoplankton backscattering coefficient ( $\text{m}^{-1}$ )
$b_{bSPIM}(\lambda)$	SPIM backscattering coefficient ( $\text{m}^{-1}$ )
$b_{bSPIM}^*(\lambda)$	SPIM specific backscattering coefficient ( $\text{m}^2 \text{g}^{-1}$ )
$b_{bw}(\lambda)$	backscattering coefficient of pure water ( $\text{m}^{-1}$ )
$b_{ph}(\lambda)$	phytoplankton total scattering coefficient ( $\text{m}^{-1}$ )
$b_w(\lambda)$	total scattering coefficient of pure water ( $\text{m}^{-1}$ )
C	an empirical constant. used in the equation defining the gamma distribution of inorganic particles
c	total attenuation coefficient ( $\text{m}^{-1}$ )
$c_{SPIM}$	is the attenuation attributed to SPIM ( $\text{m}^{-1}$ )
$c_{ph}$	is attenuation attributed to phytoplankton ( $\text{m}^{-1}$ )
$c_y$	is attenuation attributed to dissolved yellow substances ( $\text{m}^{-1}$ )
Chl	chlorophyll a + phaeophytin a concentration ( $\mu\text{g l}^{-1}$ )
$E_d$	downwelling irradiance ( $\text{w m}^{-2} \text{nm}^{-1}$ )
$E_u$	upwelling irradiance ( $\text{w m}^{-2} \text{nm}^{-1}$ )
$L_u$	upwelling radiance ( $\text{w m}^{-2} \text{nm}^{-1} \text{sr}^{-1}$ )
$L_w 0+$	water leaving radiance just above the surface ( $\text{w m}^{-2} \text{nm}^{-1} \text{sr}^{-1}$ )
PartNum	is the total particle number of a given radius
Q	the ratio $E_u / L_u$ (sr)
$Q_{scat}$	particle scattering efficiency (dimensionless)
r	is the particle radius
$r^\circ$	the frenzel coefficient for 0 degree angle of incidence which is equal to 0.021.
$R_r$	radiance reflectance ( $L_u / E_d$ )
$S_d$	shape factor for detrital absorption
SPIM	concentration of suspended particulate inorganic matter ( $\text{mg l}^{-1}$ )
SPOM	concentration of suspended particulate organic matter ( $\text{mg l}^{-1}$ )
$S_y$	shape factor for yellow substance absorption
$\beta$	a constant used in the equation defining the gamma distribution of inorganic particles having a value of -52
$\gamma$	a constant used in the equation defining the gamma distribution of inorganic particles having a value of 0.157
$\eta_w$	diffraction index of water (1.333)
$\eta_p$	diffraction index of the particle material (dimensionless) a value of 1.17 is used in the model following <i>Kirk</i> (1994)
$\mu_0$	cosine of the solar zenith angle just under the waters surface